Supporting information

Red Light-Active Porphyrin-based Zr-MOF Nanorods Enable Highly Selective Aerobic Oxidation of Sulfides and Amines

Bi-Fu Luo[1#], Xing-Yu Zhou[1#], Jin-Shan Xiong[1], Xiu-Mei Zhao[1], Xuan-Chi Zhou[1], Yu-Xiang Wang[2], Jun-Jie Zhang[1], Jiang-Feng Xin[2],Liang Xu[1], Yuan-Zhi Tan[2], Jin-Liang Zhuang[1*]*

1.School of Chemistry and Materials Science, Key Lab for Functional Materials Chemistry of Guizhou Province, Guizhou Normal University, Guiyang 550001, P. R. China. E-mail: jlzhuang@xmu.edu.cn

2. State Key Laboratory for Physical Chemistry of Solid Surfaces, and Department of Chemistry, College of Chemistry and Chemical Engineering, Xiamen University, Xiamen 361005, Fujian 550001, China. E-mail: yuanzhi_tan@xmu.edu.cn

[#] These authors contributed equally.

Table of contents

1. General methods and materials

All the chemicals were obtained from commercial sources, unless otherwise noted, and used without further purification (Innochem, J&K, TCI, and Aladdin). The sorption isotherm measurements were performed on an ASAP (Accelerated Surface Area and Porosimetry) 2020 System. Solid UV-Vis diffuse reflectance was measured by spectrometer (UV-2450) to test the absorbance (wavelength: 370~800 nm) of solid samples with barium sulfate as the substrate. The Brunauer-Emmett-Teller (BET) method was utilized to calculate the specific surface areas. The pore volume and pore size distribution were derived from the sorption curve by using the non-local density functional theory (NLDFT) model. Before gas adsorption measurement, the samples were treated with CO_2 supercritical extraction. Powder X-ray diffractions (PXRD) were recorded on a Rigaku Ultima IV diffractometer using Cu K α 1 (1.5418 Å) radiation, from 3-30°. Thermogravimetric analysis (TGA) was carried out with a NETZSCH STA449F3 in a oxygen atmosphere at a heating rate of 5 °/min. EPR spectra were measured by Bruker EMX-10/12 spectrometer at ambient temperature. SEM images were recorded using Hitachi S-4800. TEM images were obtained with a JEM-2100 microscope operated at 200 kV. FT-IR spectra were collected with a Nicolet IR 200 Fourier Transform Infrared Spectrometer at a resolution 4 cm^{-1}. GC analysis was measured on GC-9160. General GC conditions for: Restek column, 30 m × 0.32 mm × 0.5 mm; FID detector; carrier gas: N_2; area normalization. Column Conditions for a thioanisole, methyl phenyl sulfoxide, 4-fluorothioanisole, 4-chlorothioanisole, 4-bromothioanisole, 4-(methylthio)toluene, 4-methoxythioanisole, ethyl phenyl sulfide, (benzylsulfinyl)benzene, 2-(methylthio)pyridine, pentamethylene, dibutyl sulfide, amyl sulfide: 80 °C for 5 min, rising to 250 °C at a rate of 20 °C/min.

2. Experimental sections

2.1 Synthesis of 5, 10, 15, 20-tetrakis(4-carboxyphenyl) porphyrin (H_4TCPP)

5, 10, 15, 20-tetrakis(4-carboxyphenyl) porphyrin was synthesized according to previous report with modification. [1]

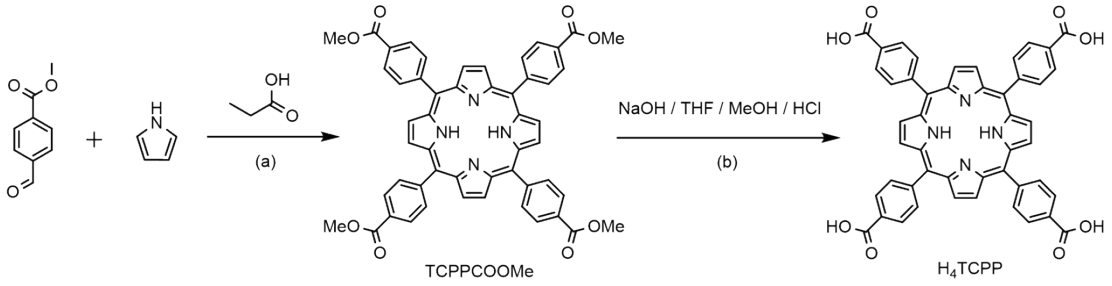

Scheme S1. Reaction conditions: (a) Propionic acid, reflux with stirring in the dark for 24 h; (b) NaOH, THF, MeOH mixed heating reflux 24 h, 1 M HCl acidification to neutral or weak acidity.

2.2 Synthesis of porphyrin-MOFs nanorods (NU-902-NR)

NU-902-NR were rapidly synthesized by a microwave-assisted method using H_4TCPP as the organic ligand, $ZrOCl_2 \cdot 8H_2O$ as the metal salt, and trifluoroacetic acid as the modifier for 10 min. The specific synthesis process was as follows: $ZrOCl_2 \cdot 8H_2O$ (20.30 mg, 0.063 mmol) and benzoic acid (BA) (138.16 mg, 1.135 mmol) were weighed in a 20 mL glass vial, dissolved by ultrasonication in 3 mL of DMF, and then placed in an oven at 80 °C for 1 h to produce Zr-oxo cluster precursor solution, which was cooled to room temperature. Weigh the tetracarboxylic acid organic ligand H_4TCPP (3.95 mg, 0.005 mmol) and add 1 mL of DMF ultrasonication dissolved in the above precursor solution, and add 20 μL CF_3COOH, ultrasonication for 10 min to make the system dispersed, and then put into a domestic microwave oven (M1-L213B) in the "Medium-low" mode for 10 min. After cooling, the dark brown solid was collected by

centrifugation and washed twice with DMF and twice with EtOH, and then freeze-dried for 24 h for activation.

2.3 Catalytic studies of NU-902-NR

2 mg NU-902-NR was used as the photocatalyst and 0.3 mmol sulfide was added into a cocktail flask containing 2 mL of oxygen-saturated solvent, sealed and inserted with an oxygen bulb, dispersed by sonication in the dark, irradiated with a 3W LED lamp (blue/425 nm, green/520 nm, red/625 nm), and stirred to the set reaction time at room temperature. At the end of the reaction, the catalyst was separated by centrifugation, the aqueous phase was collected and extracted by adding a small amount of DCM, and then the organic layer was collected and dried by adding anhydrous $NaSO_4$, the liquid was collected by filtration and added with an internal standard (nitrobenzene), and the composition of the supernatant was analyzed by using a GC-9160, and the conversion of sulfur ether to sulfoxide was calculated from the peak area to determine the conversion and selectivity.

2.4 Gram-scale synthesis of 1-(methylsulfinyl)-4-methoxybenzene under red LED and 4-Bromophenylmethylsulfoxide under sunlight

Gram-scale photocatalytic oxidation reactions were carried out using NU-902-NR (20 mg) as the catalyst under both red LED and natural sunlight irradiation. In a typical procedure, 1-(methylsulfanyl)-4-methoxybenzene (1.5 g, 10 mmol) was dissolved in 100 mL of H_2O in a quartz reactor, and molecular oxygen (O_2) was continuously introduced using a balloon as the oxidant source. The suspension was irradiated with a red LED (3 W, 625 nm) under magnetic stirring for 6 h at room temperature. After completion of the reaction, the catalyst was removed by simple filtration, and the solvent was evaporated under reduced pressure using a rotary evaporator to afford 1.4

g of 1-(methylsulfinyl)-4-methoxybenzene as a faint yellow solid product (Yield: 93%, Selectivity: 97%).

For the sunlight-driven reaction, the same catalytic system was used with 4-bromothioanisole (2.0 g, 10 mmol) as the substrate. The reaction mixture was exposed to natural sunlight (10:00 a.m.–5:00 p.m.) under O_2 atmosphere with continuous stirring. After reaction, the catalyst was separated by filtration and the solvent was removed by rotary evaporation to give 1.8 g of 4-bromophenylmethylsulfoxide as a light-yellow powder (Yield: 90%, Selectivity: 98%).

2.5 Quantification of superoxide radical ($O_2^{\bullet-}$) via the nitroblue tetrazolium (NBT) reduction assay

The concentration of $O_2^{\bullet-}$ was quantified using the nitroblue tetrazolium (NBT) photoreduction method, based on the specific reaction between $O_2^{\bullet-}$ and NBT to form an insoluble purple formazan precipitate. Under air-saturated conditions, the photocatalytic activity of NU-902-NR was evaluated using either blue LED (3 W) or red LED (3 W) as the excitation source. A series of catalysts (1, 2, 5 and 10 mg) were dispersed in 30 mL of a 1 mM NBT aqueous solution containing 540 μL of methyl phenyl sulfide, followed by magnetic stirring in the dark for 30 min to establish adsorption-desorption equilibrium. The suspension was then irradiated for 60 min. After the reaction, the mixture was filtered through a 0.22 μm membrane to remove the catalyst and the formed precipitates. The filtrate was analyzed using UV-vis spectroscopy at 259 nm to monitor the decrease in NBT absorbance, from which the amount of $O_2^{\bullet-}$ generated was determined.

2.6 The selective oxidation experiment of α-terpinene by NU-902-NR

In a typical procedure, 0.1 mmol of α-terpinene was added to a reaction vial containing 2 mg of NU-902-NR as the photocatalyst and 2 mL of O_2-saturated acetonitrile. The

vial was sealed, fitted with an O_2 balloon, and sonicated in the dark to ensure thorough dispersion. The suspension was then irradiated with a 3 W LED light source (blue, 425 nm; red, 625 nm) for 3 h. After irradiation, the catalyst was removed by centrifugation, and the resulting organic phase was collected and analyzed by GC-MS to determine the reaction product.

2.7 Computational details

All geometric structures were optimized using the DFT based Dmol^3 method, using the generalized gradient approximation with Perdew-Burke-Ernzerhof exchange-correlation functional (GGA-PBE) [2,3]. For Zr element, the core electrons were replaced by the density functional semicore pseudopotential (DSPP) [4], whereas C, H, O, and N element were treated as in the all-electron case. For the valence electron wave function of atoms, the doubled numerical plus polarization (DNP) [5] basis sets were adopted, namely, GGA-PBE/DNP, DSPP.

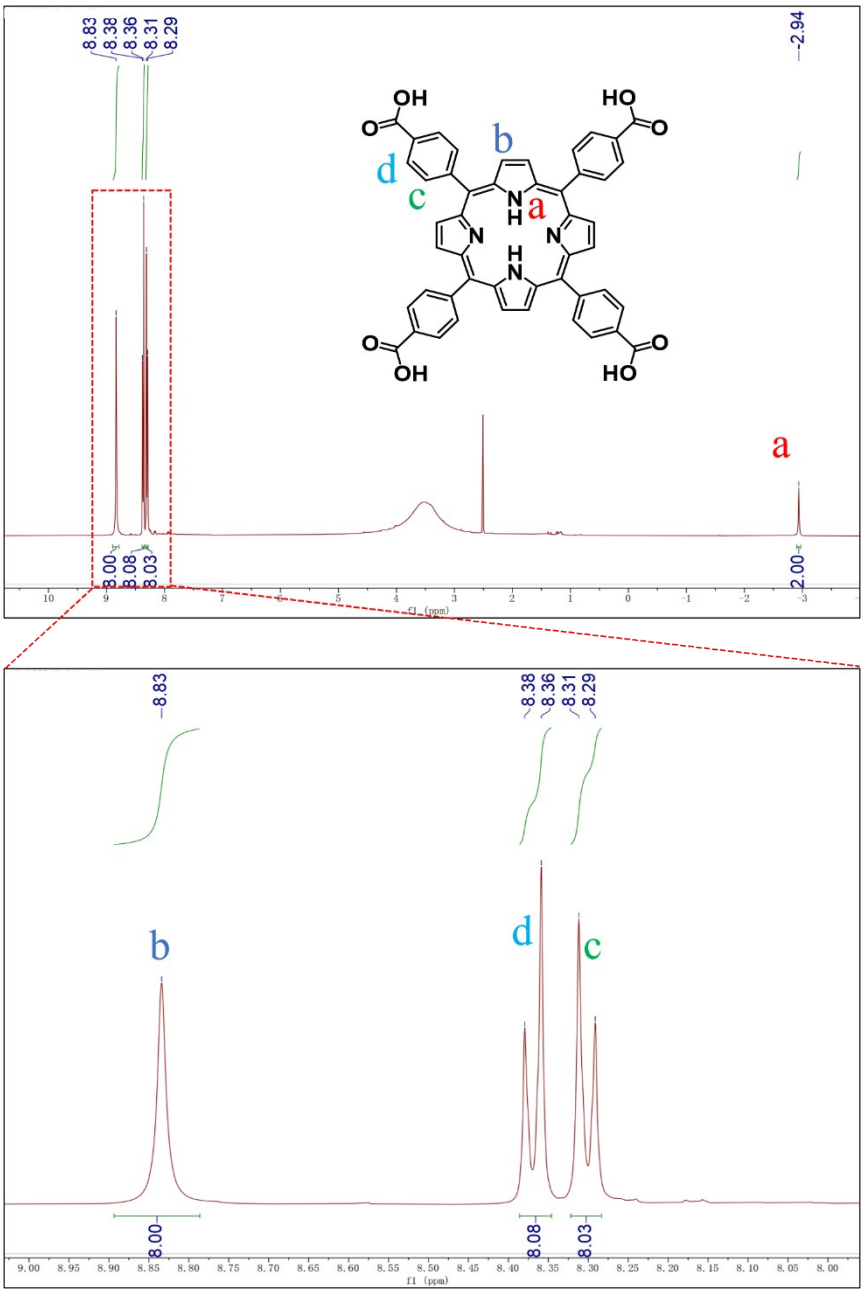

Fig. S1. ^{1}H-NMR spectrum of H_4TCPP in DMSO-d_6. The synthesized H_4TCPP is a purple crystal. ^{1}H NMR (400 MHz, DMSO-d_6) δ 8.83 (s, 8H), 8.37 (d, J = 8.4 Hz, 8H), 8.30 (d, J = 8.3 Hz, 8H), -2.94 (s, 2H).

3. Characterizations of NU-902 nanorods

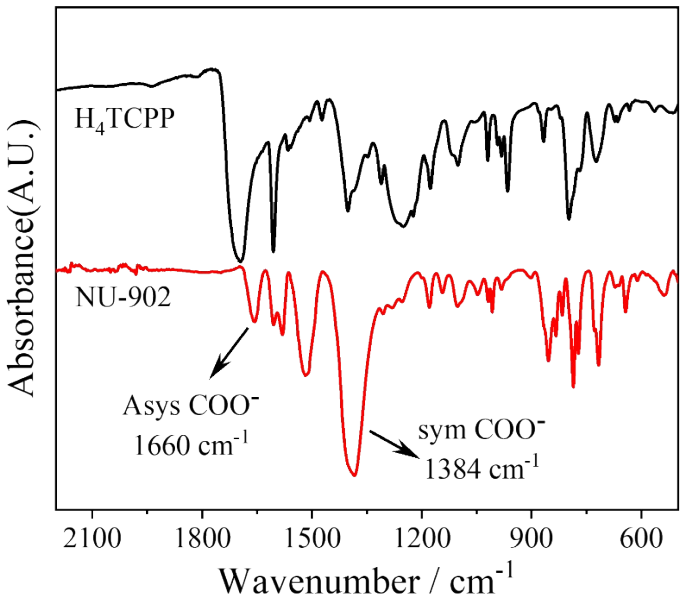

Fig. S2. FTIR spectra of the organic ligand H_4TCPP (black) and as-synthesized NU-902-NR (red). The -C=O vibrational peak of H_4TCPP at 1700 cm^{-1} essentially disappears in the NU-902 nanorods and is replaced by symmetric and asymmetric telescoping vibrational peaks of -COO at 1410 and 1600 cm^{-1}, which proves the coordination between the porphyrin-COOH and $Zr_6(\mu\text{-}OH)_8$.

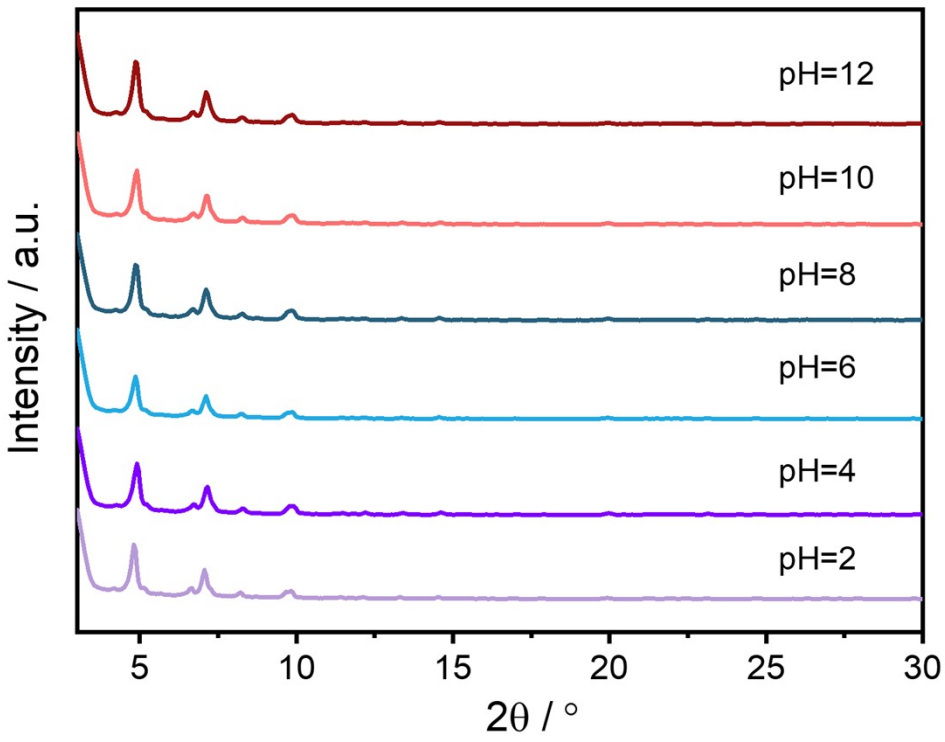

Fig.S3. XRD patterns of NU-902-NR under different pH conditions.

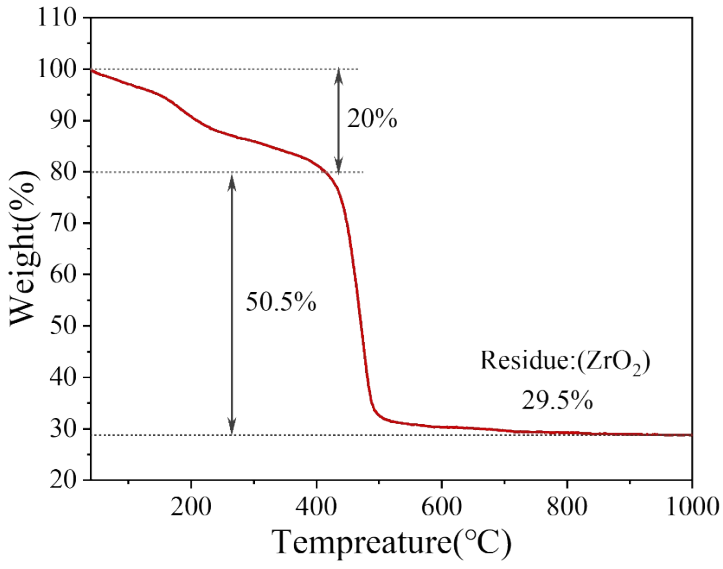

Fig. S4. Thermogravimetric analysis (TGA) curve of NU-902-NR under air. The NU-902-NR is thermally stable up to 500 °C in an O_2 atmosphere.

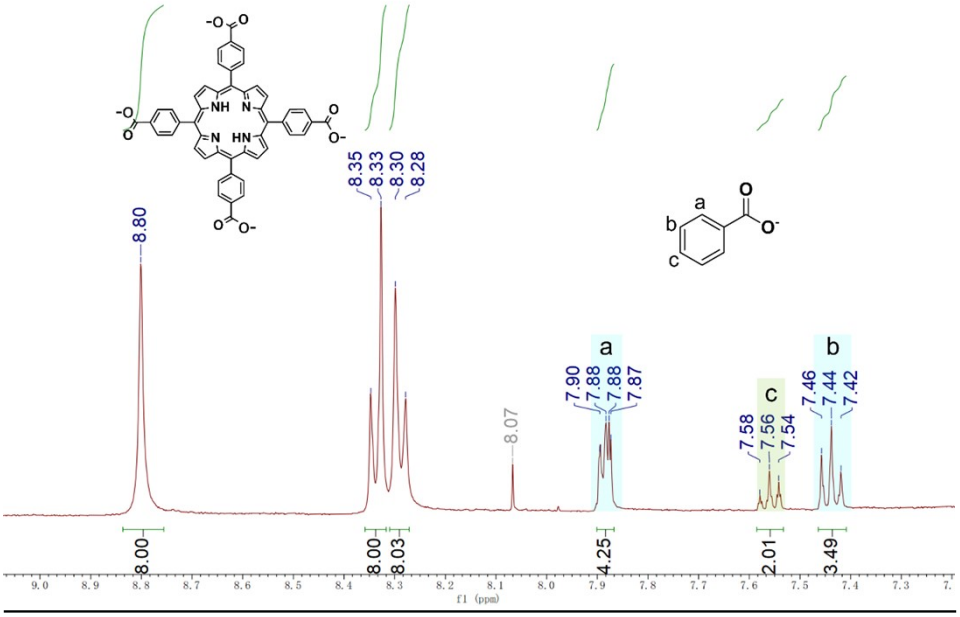

Fig. S5. ^{1}H NMR spectra of NU-902-NR digested in DMSO-d_6. Digestion was performed by dispersing 5 mg of NU-902-NR powder (preactivated in CH_3OH and vacuum for 12 hours) in 0.6 mL DMSO-d_6 and 20 µL HF. [6]

Calculations of linker missing defects from TGA (under O_2) profiles. Semiquantitative analysis of TGA data is based on the assumption that the residue is pure ZrO_2. To ensure this, the TGA measurements were carried out under a flow of an oxygen stream and temperature run up to 1000 °C. In order to minimize the effect of entrapped solvent (e.g., H_2O, ethanol), DSC (differential scanning calorimetry) data was used to define the initial temperature of solvent free samples. For an ideal sample, the molar mass of $[Zr_6(\mu_3\text{-}O)_4(\mu_3\text{-}OH)_4(OH)_4(OH_2)_4(TCPP)_2(BA)_4]$ is 2879.8 g/mol. The complete combustion of sample will result in 6*ZrO_2, which has total molar mass 739.2 g/ mol (6*123.2). Therefore, the residue plateau should ideally be found in 25.6% (739.2/2879.8) in TGA profiles. Assuming that the defects are caused by linker missing, the amount of ZrO_2 is the same as perfect crystals, but the total molar mass of crystal will be lower than perfect one, which results in higher percentage of ZrO_2 in TGA

profiles. In our experiments, we found that the residue plateau is 29.5%, resulting in 0.5 TCPP linker missing per node (calculations see following).

For NU-902-NR:

$$\frac{6 \times ZrO_2}{[Zr_6(O)_4(OH)_4(OH)_4(OH_2)_4(BA)_4]TCPP_{(2-x)}} = \frac{6 \times 123.2}{2879.8 - 786.7x} = 29.5\%$$

x=0.5 was the number of missing linker.

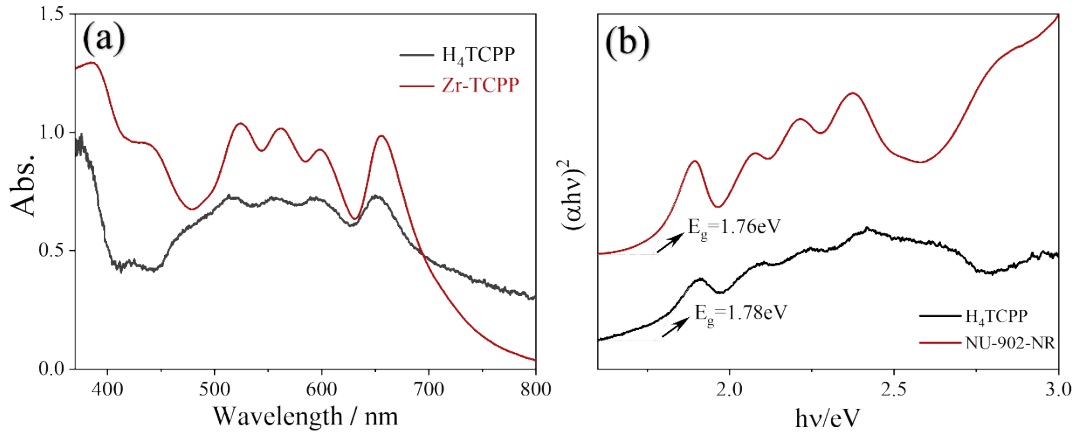

Fig. S6. (a) UV-Vis-DRS spectrum of H_4TCPP (red) and NU-902-NR (black); (b) Spectrogram of $(\alpha h\nu)^2$-hν of H_4TCPP (red) and NU-902-NR (black).

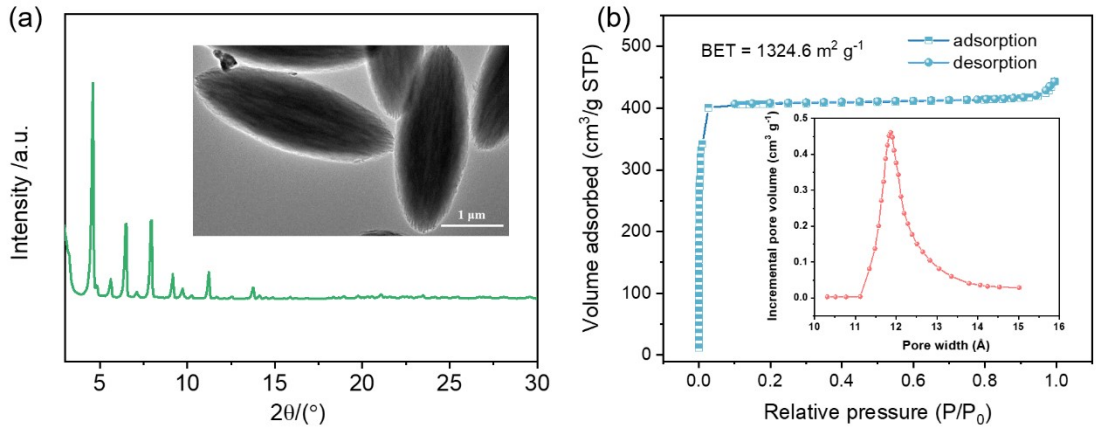

Fig. S7. (a) PXRD pattern of bulk NU-902, inset is the TEM image of bulk NU-902. (b) N_2 adsorption-desorption isotherms of bulk NU-902-bulk (inset shows the pore size distribution).

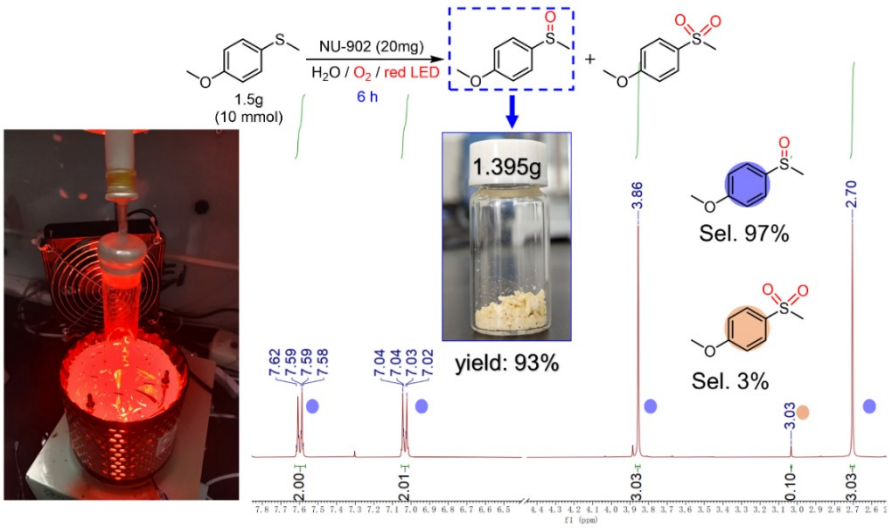

Fig. S8. Photograph of the red light-mediated photosynthesis of (4-methoxyphenyl) (methyl)sulfane in a gram-scale; ^{1}H NMR spectrum indicates that the selectivity of target product is 97%. ^{1}H NMR (400 MHz, $CDCl_3$) δ 7.62-7.58 (d, 2H, Ar), 7.04-7.02 (d, 2H, Ar), 3.86 (s, 3H, -O-CH_3), 2.70 (s, 3H, -CH_3). Note: for clarity, only one of the characteristic ^{1}H NMR peak (-SO_2-CH_3) belongs to sulfone by-product was marked.

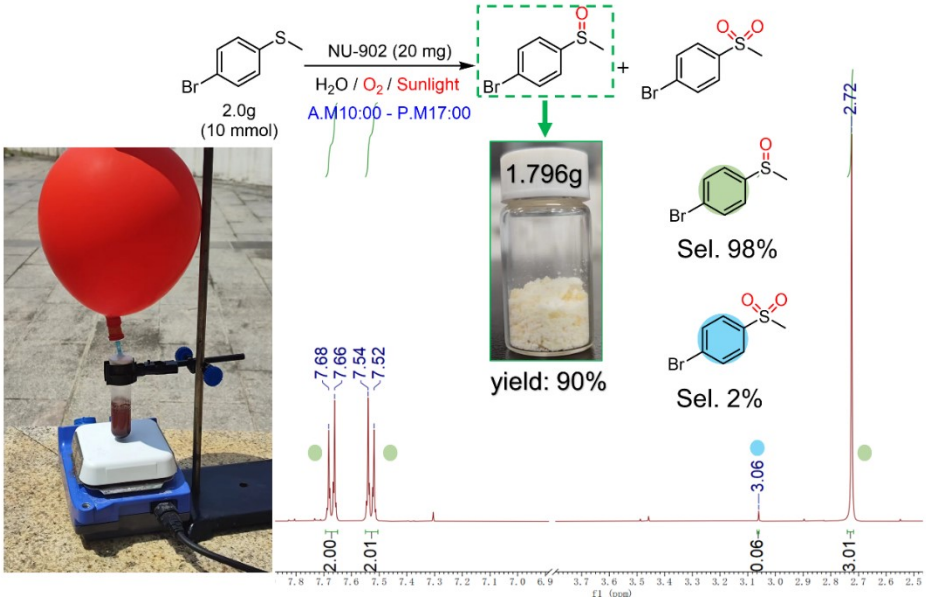

Fig. S9. Photograph of the nature sun light-mediated photosynthesis of 1-bromo-4-(methylsulfinyl)benzene in a gram-scale; ^{1}H NMR spectrum indicates that the selectivity of target product is 98%. ^{1}H NMR (400 MHz, $CDCl_3$) δ 7.67 (d, 2H, Ar),

7.53 (d, 2H, Ar), 2.72 (s, 3H, CH_3). Note: for clarity, only one of the characteristic ^{1}H NMR peak (-SO_2-*CH_3*) belongs to sulfone by-product was marked.

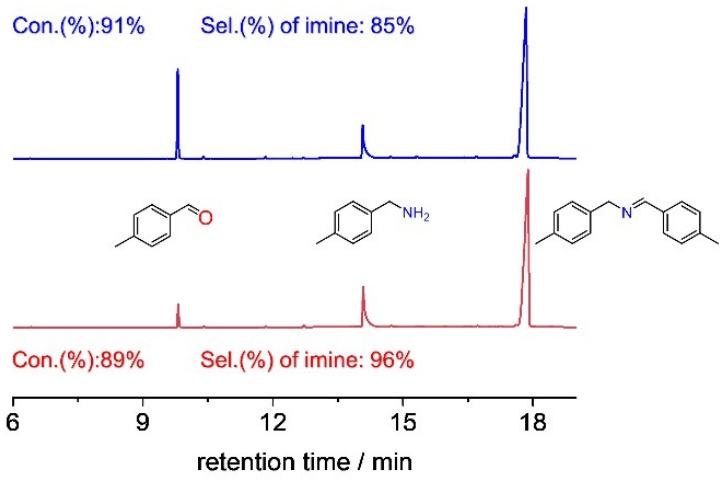

Fig. S10. GC results of photooxidation of 4-methylbenzylamine catalyzed by NU-902-NR under red light (down, red curve) and blue light (top, blue curve) irradiation.

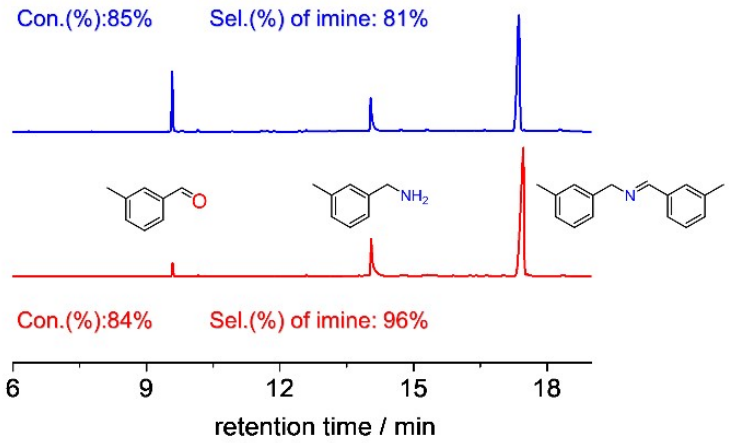

Fig. S11. GC results of photooxidation of 3-methylbenzylamine catalyzed by NU-902-NR under red light (down, red curve) and blue light (top, blue curve) irradiation.

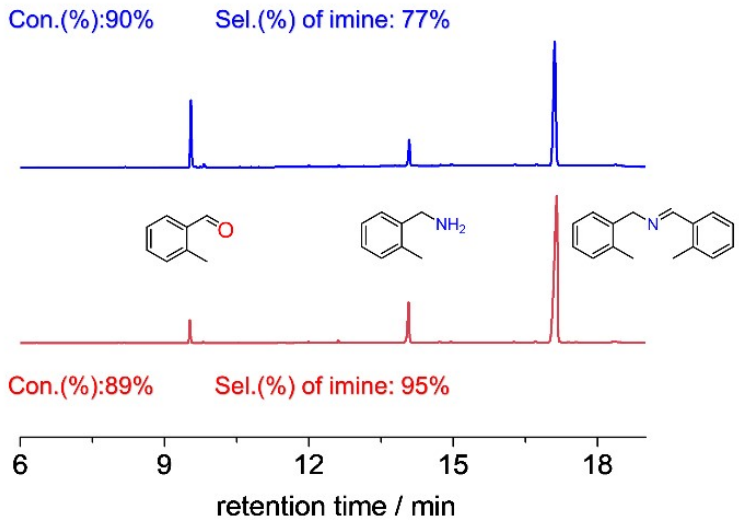

Fig. S12. GC results of photooxidation of 2-methylbenzylamine catalyzed by NU-902-NR under red light (down, red curve) and blue light (top, blue curve) irradiation.

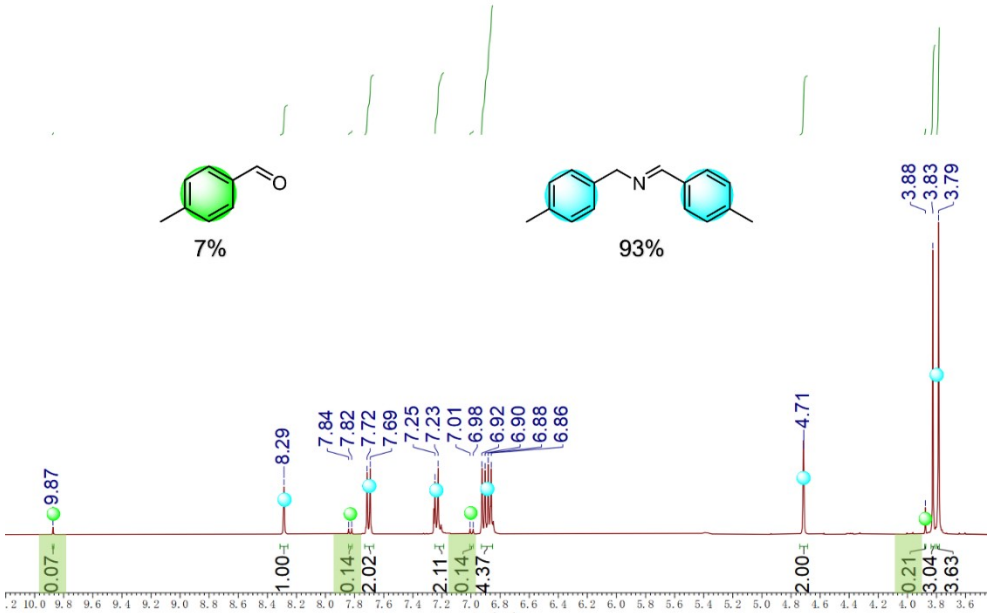

Fig. S13. [1]HNMR spectrum of targeted (E)-N-(4-methylbenzyl)-1-(p-tolyl)methanimine (selectivity: 93%) and p-tolualdehyde as side product (7%) under red light irradiation.

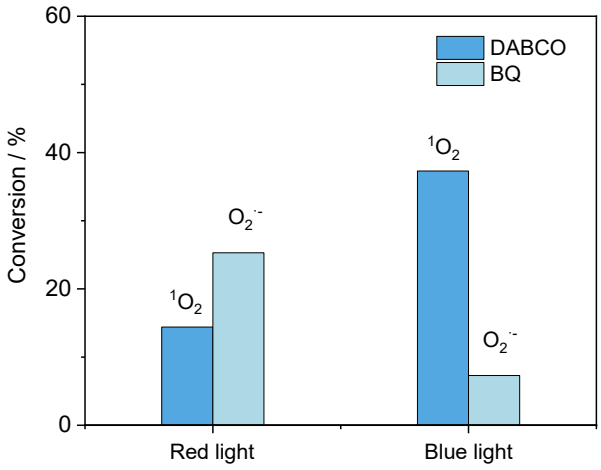

Fig. S14. Conversions of the 4-methylbenzylamine coupling reaction in the presence of different reactive oxygen species (ROS) scavengers under blue light and red-light irradiation. DABCO was employed as a $^1O_2$ quencher, while BQ served as an $O_2^{\bullet-}$ scavenger.

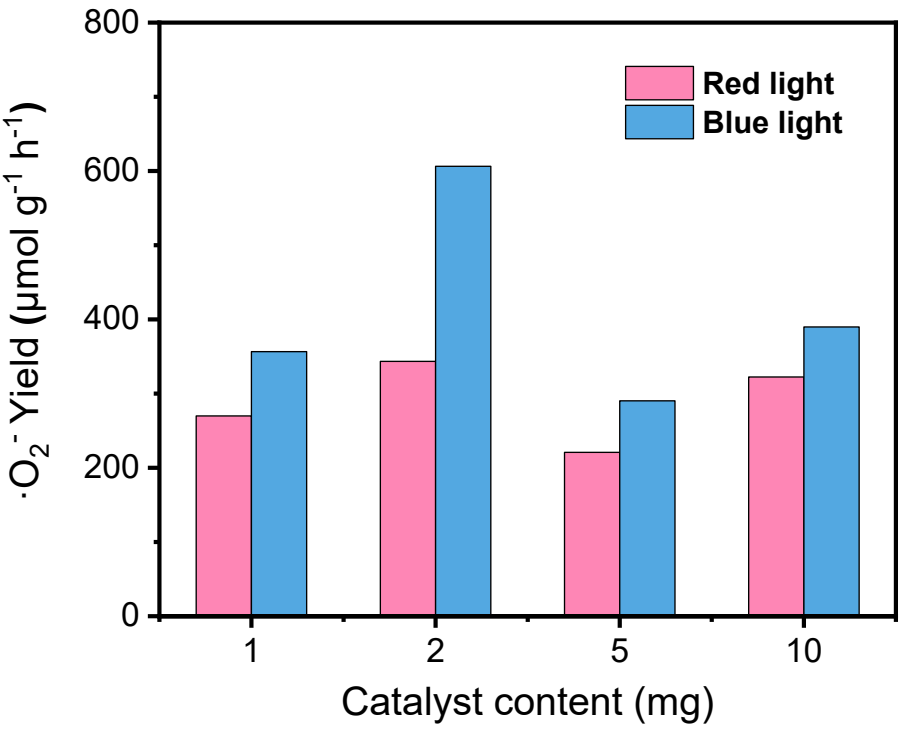

Fig. S15. Quantitative analysis of $O_2^{\bullet-}$ generation under red and blue light irradiation using nitroblue tetrazolium (NBT) as the probing reagent. $O_2^{\bullet-}$ yields (μmol g^{-1} h^{-1})

were measured at different catalyst dosage.

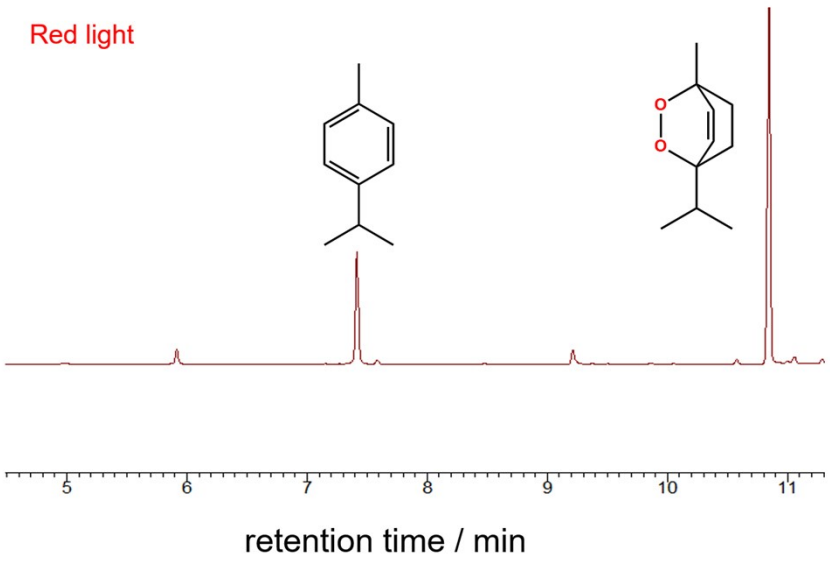

Fig. S16. GC results of photooxidation of α-terpinene catalyzed by NU-902-NR under red light irradiation.

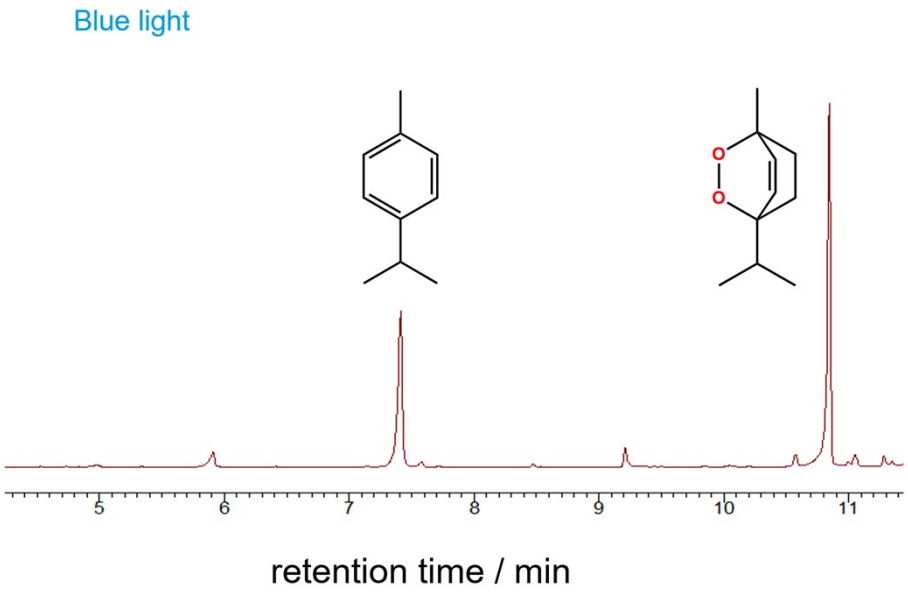

Fig. S17. GC results of photooxidation of α-terpinene catalyzed by NU-902-NR under blue light irradiation.

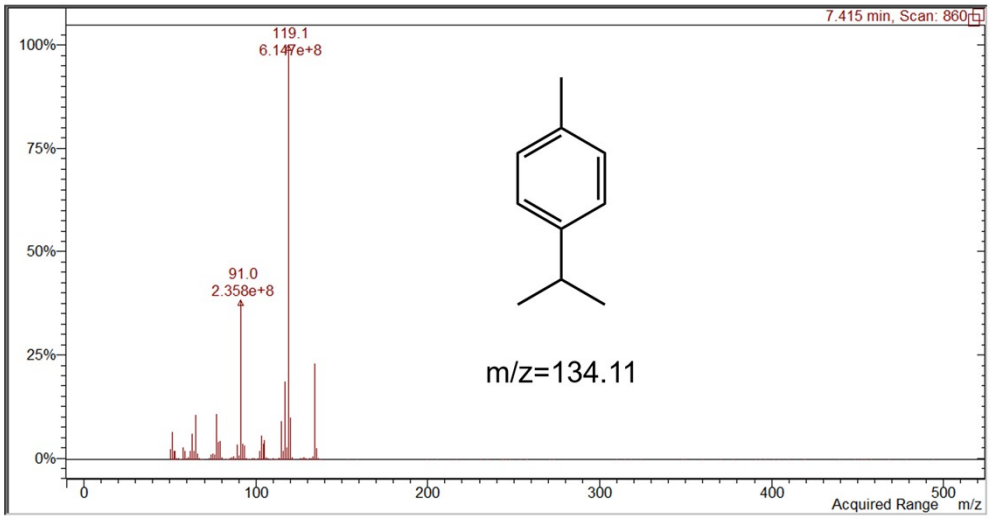

Fig. S18. MS spectrum of the oxidation product of 4-isopropyltoluene catalyzed by NU-902-NR under red light irradiation.

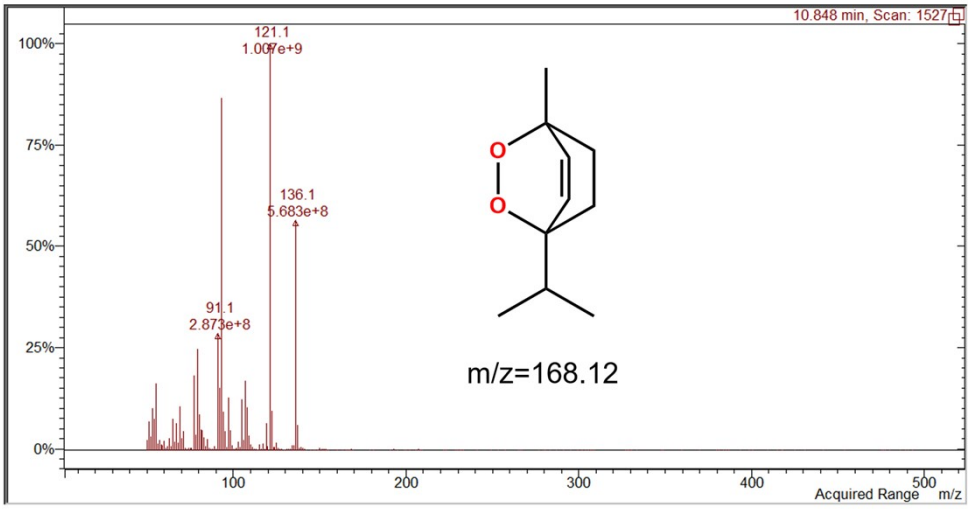

Fig. S19. MS spectrum of the oxidation product of ascaridole catalyzed by NU-902-NR under red light irradiation.

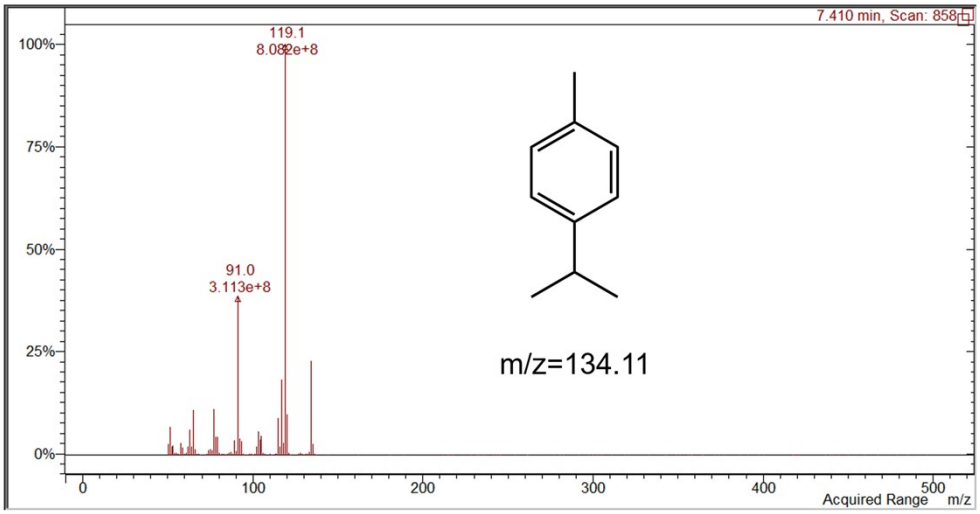

Fig. S20. MS spectrum of the oxidation product of 4-isopropyltoluene catalyzed by NU-902-NR under blue light irradiation.

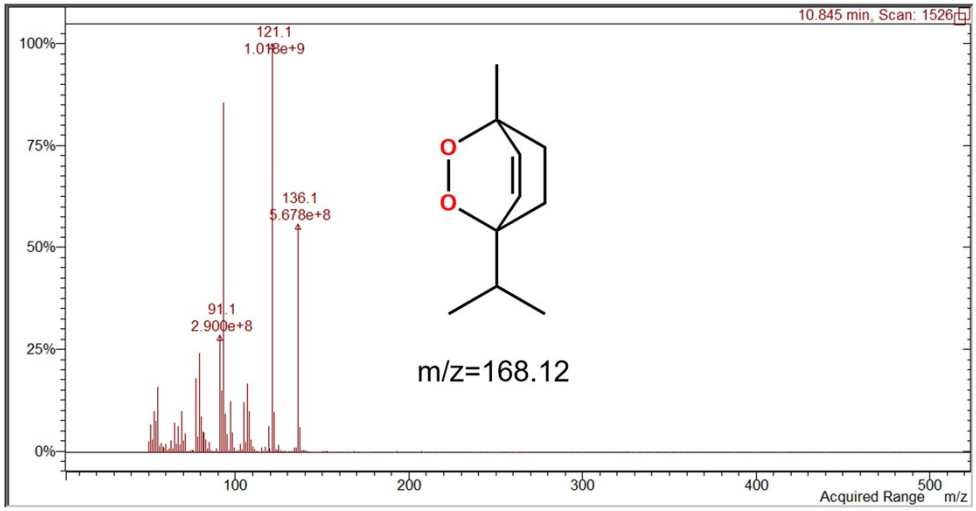

Fig. S21. MS spectrum of the oxidation product of ascaridole catalyzed by NU-902-NR under blue light irradiation.

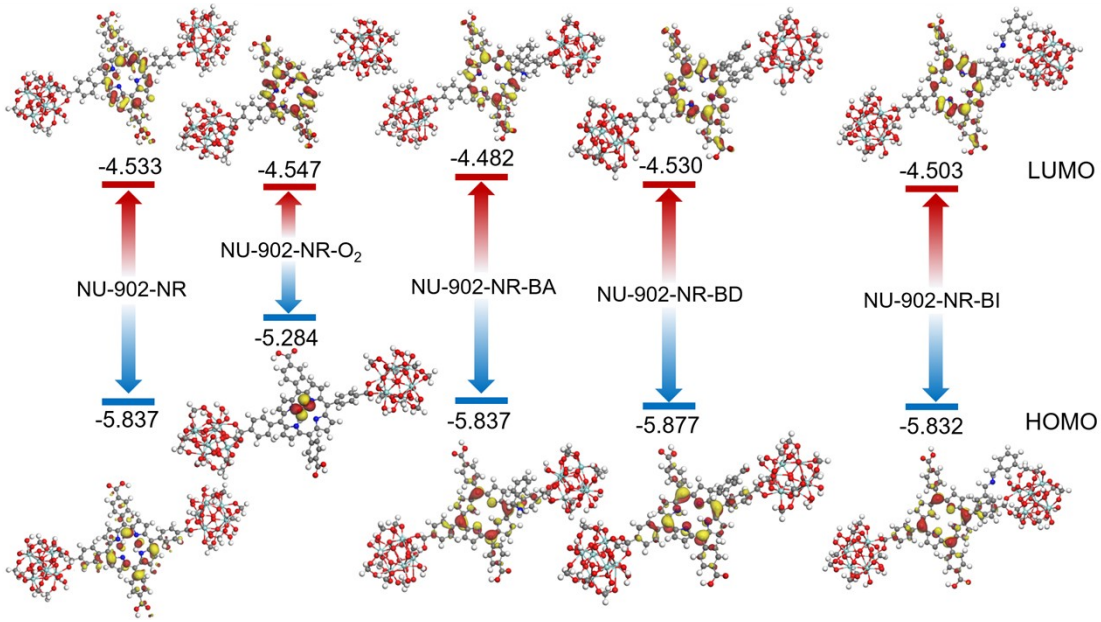

Fig. S22. HOMO-LUMO energy levels of NU-902-NR and its substrate- or intermediate-bound states (NU-902-NR-O_2, NU-902-NR-BA, NU-902-NR-BD, and NU-902-NR-BI). The calculated HOMO-LUMO energies reveal the electronic variations associated with O_2 adsorption, benzylamine (BA) binding, benzaldehyde (BD) formation, and N-benzylidene benzylamine (BI) generation.

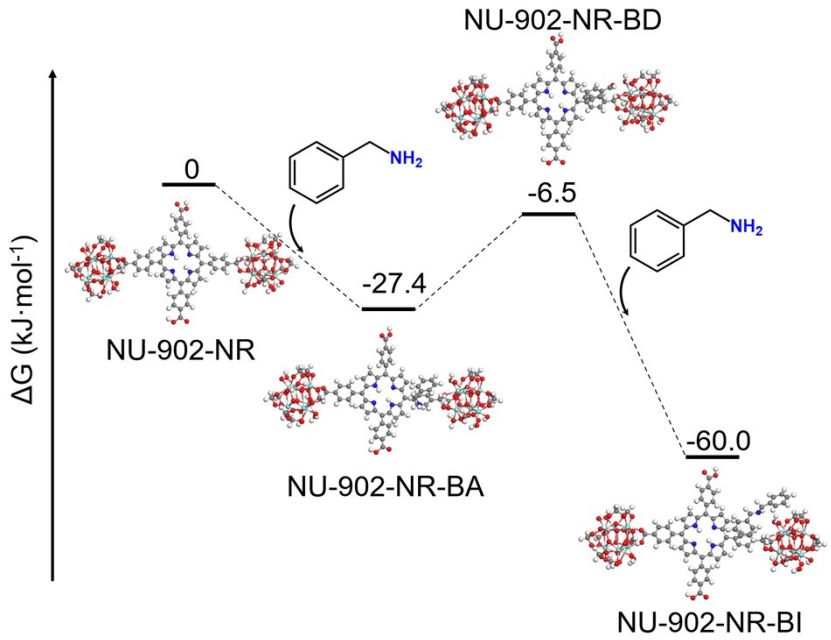

Fig. S23. Energy profiles involved in the oxidation of benzylamines by NU-902-NR catalyst (BA, benzylamine; BD, benzaldehyde; BI, N-benzylidene benzylamine) .

Table S1. Comparison of photooxidation of thioanisole over various reported catalysts.

No.	Catalyst	Light	Solvent	Time (h)	Con. (%)	Sel. (%)	Catalyst loading	Ref.
1	NU-902-NR	Red(3W)	H_2O	3	98	>99	2 mg	This work
2	Bulk NU-902	Red(3W)	H_2O	3	90	95	2 mg	-
3	PCN-222	Red	CH_3OH, HOOC-TEMPO	0.25	85	98	5 mg	[7]
4	Hf-NU-1000	Blue(3 W) ×4	CH_3OH, HOOC-TEMPO	0.42	96	91	5 mg	[8]
5	NU-1100	Green	CH_3OH. 4-HOOC-TEMPO	0.67	66	97	5 mg	[9]
6	PMOF (Ti)	Red(3 W) ×4	CH_3OH	0.75	94	100	5 mg	[10]
7	TPPS-BV	LED (420-750 nm)	CH_3OH	1	>99	>99	10 mg	[11]
8	$Zn_2(BODIPY)_2(TDC)_2$	Blue (16W)	$CH_3OH/CHCl_3$	1.5	99	99	3 mg	[12]
9	C_{60}@PCN-222	LED (λ > 400 nm)	CH_3OH	3	>99	>99	20 mg	[13]
10	UiO-68-A-D-A	Blue (30 W)	CH_3CN	7	99	99	1 mmol	[14]
11	I_2-BODIPY@ZIF-8	Green	CH_3OH	7	99	99	20 mg	[15]
12	PCN-2001	Xe lamp (300 W)	H_2O	8	>99	>99	20 mmol	[16]
13	Zr-TCA	Blue (24W)	CH_3OH	10	100	98	20 mmol	[17]
14	UiO-66(Ce)-2A	Xe lamp (λ > 400 nm)	CH_3CN	14	98.4	>99	20 mg	[18]
15	Ni-PBA-Th_6	Full spectrum	CH_3OH/H_2O_2	48	>99	>97	20 mg	[19]

^{1}H NMR spectra of some products

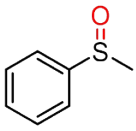

(methylsulfinyl)benzene: ^{1}H NMR (400 MHz, $CDCl_3$) δ 7.72-7.69 (m, 2H, Ar), 7.62-7.57 (m, 3H, Ar), 2.78 (s, 3H, CH_3).

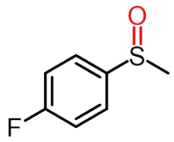

1-fluoro-4-(methylsulfinyl)benzene: ^{1}H NMR (400 MHz, $CDCl_3$) δ 7.67 (d, 2H, Ar), 7.24 (d, 2H, Ar), 2.73 (s, 3H, CH_3).

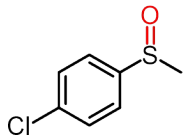

1-Chloro-4-(methylsulfinyl)benzene: ^{1}H NMR (400 MHz, $CDCl_3$) δ 7.60 (d, 2H, Ar), 7.51 (d, 2H, Ar), 2.73 (s, 3H, CH_3).

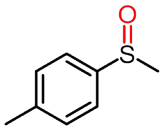

1-methyl-4-(methylsulfinyl)benzene: ^{1}H NMR (400 MHz, $CDCl_3$) δ 7.54 (d, 2H, Ar), 7.33 (d, 2H, Ar), 2.71 (s, 3H, CH_3), 2.41 (s, 3H, CH_3).

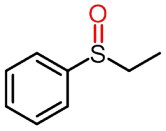

(ethylsulfinyl)benzene: ^{1}H NMR (400 MHz, $CDCl_3$) δ 7.63-7.60 (m, 2H, Ar), 7.57 - 7.46 (m, 3H, Ar), 2.97-2.74 (m, 2H, CH_2), 1.20 (m, 3H, CH_3).

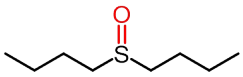

1-(butylsulfinyl)butane: ^{1}H NMR (400 MHz, $CDCl_3$) δ 2.76 - 2.59 (m, 4H, CH_2), 1.82-1.70 (m, 4H, CH_2), 1.59-1.41 (m, 4H, CH_2), 0.97 (t, 6H, CH_3).

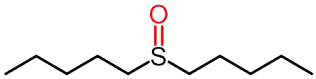

1-(pentylsulfinyl)pentane: ^{1}H NMR (400 MHz, $CDCl_3$) δ 2.75-2.58 (m, 4H, CH_2), 1.88-1.70 (m, 4H, CH_2), 1.53-1.34 (m, 4H, CH_2), 0.92 (t, 6H, CH_3).

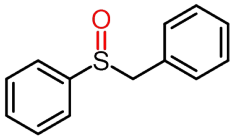

(benzylsulfinyl)benzene: ^{1}H NMR (400 MHz, DMSO) δ 7.46-7.40 (m, 3H, Ar), 7.39-7.36 (m, 2H, Ar), 7.29-7.22 (m, 3H, Ar), 6.99-6.97 (m, 2H, Ar), 4.11-3.98 (d, 2H, CH_2).

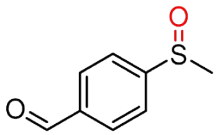

4-(methylsulfinyl)benzaldehyde: ^{1}H NMR (400 MHz, $CDCl_3$) δ 10.10 (s, 1H, CHO), 8.05 (d, 2H, Ar), 7.83 (d, 2H, Ar), 2.79 (s, 3H, CH_3).

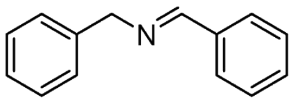

(E)-N-benzyl-1-phenylmethanimine: ^{1}H NMR (400 MHz, $CDCl_3$) δ 8.38 (s, 1H, CH), 7.78-7.77(m, 2H, Ar), 7.41-7.34 (m, 3H, Ar), 7.33-7.24 (m, 5H, Ar), 4.82 (s, 2H, CH_2).

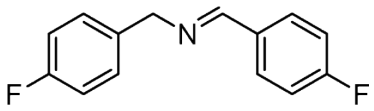

(E)-N-(4-fluorobenzyl)-1-(4-fluorophenyl)methanimine: ^{1}H NMR (400 MHz, $CDCl_3$) δ 8.34 (s, 1H, CH), 7.78-7.75 (m, 2H, Ar), 7.31-7.25 (m, 2H, Ar), 7.12-7.07 (m, 2H, Ar), 7.05-7.00 (m, 2H, Ar), 4.76 (s, 2H,CH_2).

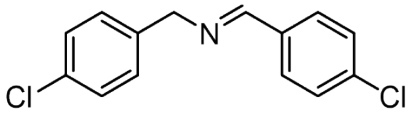

(E)-N-(4-chlorobenzyl)-1-(4-chlorophenyl)methanimine: ^{1}H NMR (400 MHz, $CDCl_3$) δ 8.33 (s, 1H, CH), 7.71 (d, 2H, Ar), 7.38 (d, 2H, Ar), 7.31 (d, 2H, Ar), 7.29-7.21 (m, 2H, Ar), 4.76 (s, 2H, CH_2).

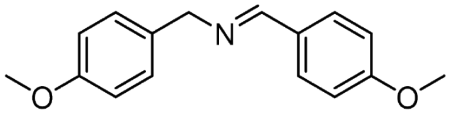

(E)-N-(4-methoxybenzyl)-1-(4-methoxyphenyl)methanimine: ^{1}H NMR (400 MHz, $CDCl_3$) δ 8.29 (s, 1H, CH), 7.70 (d, 2H, Ar), 7.24 (d, 2H, Ar), 6.92-6.86 (m, 4H, Ar), 4.71 (s, 2H, CH_2), 3.83 (s, 3H, CH_3), 3.79 (s, 3H, CH_3).

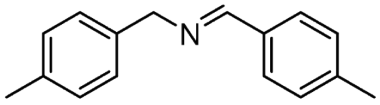

(E)-N-(4-methylbenzyl)-1-(p-tolyl)methanimine: ^{1}H NMR (400 MHz, $CDCl_3$) δ 8.33 (s, 1H, CH), 7.65 (d, 2H, Ar), 7.23 (m, 4H, Ar), 7.14 (d, 2H, Ar), 4.75 (s, 2H, CH_2), 2.37 (s, 3H, CH_3), 2.33 (s, 3H , CH_3).

References:

[1] E. Y. Jeong, M. B. Ansari, Y. H. Mo, S. E. Park, *J. Hazard. Mater*. 2011, **185,** 1311-1317.

[2] Perdew, J. P.; Burke, K.; Ernzerhof, M. *Phys. Rev. Lett.* 1996, 77, 3865−3868.

[3] Delley, B. *Rev. B.* 2002, **66,** 155125.

[4] Delley, B. *J. Chem. Phys.* **1990,** 92, 508−517.

[5] Rappé, A. K.; Casewit, C. J.; Colwell, K. S.; Goddard III, W. A.; Skiff, W. M. UFF. J. *Am. Chem. Soc.* **1992,** 114, 10024−10035.

[6] P. Deria, J. Yu, R.P. Balaraman, J. Mashni, S.N. White, *Chem. Commun.* 2016, **52,** 13031-13034.

[7] W. Sheng, X. Wang, Y. Wang, S. Chen and X. Lang, *ACS Catal.*, 2022, **12**, 11078-11088.

[8] B. Zeng, W. Sheng, F. Huang, K. Zhang, K. Xiong and X. Lang, *Chem. Eng. J.*, 2023, **474**, 145559.

[9] B. Zeng, F. Huang, Y. Wang, K. Xiong and X. Lang, *Chin. J. Catal.*, 2024, **58**, 226-236.

[10] W. Sheng, H. Hao, F. Huang, F. Zhang and X. Lang, *Chem. Eng. J.*, 2022, **430**, 133071.

[11] B. Cai, P. Huang, Y. Fang and H. Tian, *Adv. Sci.*, 2024, **11**, 2308469.

[12] Q. Kang, S.-D. Wang, J. Guo, K.-L. Mo, K.-L. Lv and L.-L. Wen, *Inorg. Chem. Front.*, 2024, **11**, 4731-4739.

[13] D.-Y. Zheng, E.-X. Chen, C.-R. Ye and X.-C. Huang, *J. Mater. Chem. A*, 2019, **7**, 22084-22091.

[14] M. Shao, H. Guo, R. Bao, C. Liu, C. Yao, Y. Song and X. Guo, *Chem. Eng. J.*, 2025, **515**, 163233.

[15] J. F. Zhou, J. J. Ling, G. Li, S. Zhang and D. Zhu, *Mater. Today Chem.*, 2022, **24**, 100774.

[16] H.-H. He, Z.-J. Guan, J.-P. Yuan, Y.-Y. Zhao, H. Zhang, W. Gong, L.-L. Zhang, Y. Yan and Y. Fang, *CCS Chem.*, 2025, 1-36.

[17] D. Zhang, X.-N. Zou, X.-G. Wang, J. Su, T.-X. Luan, W. Fan, P.-Z. Li and Y. Zhao, *ACS Appl. Mater. Interfaces*, 2022, **14**, 23518-23526.

[18] C. Liu, Y.-Z. Shi, Q. Chen, B.-H. Ye, J.-H. Bi, J. C. Yu and L. Wu, *Rare Met.*, 2025, **44**, 2462-2473.

[19] X. F. Li, P. Wu, L. Kan, Q. Niu, S. N. Sun, Q. Huang and Y. Q. Lan, *Adv. Funct. Mater.*, 2023, **33**, 2308534.